Nuclear Engineering and Design/Fusion 2 (1985) 97–110
North-Holland, Amsterdam

DEVELOPMENT OF DESIGN EQUATIONS FOR FERRITIC ALLOYS IN FUSION REACTORS

Robert J. AMODEO and Nasr M. GHONIEM

Fusion Engineering and Physics group, School of Engineering and Applied Science, University of California at Los Angeles, Los Angeles, CA 90024, USA

Received 16 February 1984

Several methods for developing design correlations for ferritic steels are discussed in this paper. Equations which describe swelling, embrittlement, and irradiation creep are reviewed. We develop design equations for use in inelastic structural mechanics applications, for the most important thermal creep parameters. Empirical correlations for creep rupture time and the complete description of elongation vs. time are presented. A phenomenological description of steady-state creep is also developed.

1. Introduction

The need for design equations stems from current interest in determining the lifetime of materials in the fusion environment [1]. Equations which describe the swelling, embrittlement and thermal creep for a given metal can define an effective irradiation temperature-operation lifetime window. The ferritic steels in particular have been considered as possible candidates for fusion applications for the following reasons:

1. Ferritic and Martensitic steels exhibit great resistance to void swelling under neutron bombardment.
2. The thermal stress resistance is greater than austenitic alloys allowing the use of thicker sections for first wall applications.
3. Limited evidence indicates that helium generation by neutron irradiation may not significantly degrade the mechanical properties [2,3].

These characteristics are important because the phenomena induced by irradiation cover a wide range of temperatures. Under the normal operation of fusion reactors, startup, shutdown and burn modes, such a temperature range is encountered. It is therefore necessary to assess the viability of utilizing ferritic alloys in fusion reactors by developing design equations which are good for operating temperature ranges. The main difficulty encountered in determining accurate design equations is the limited amount of available data on design related phenomena. The purpose of this paper is not only to provide current versions of equations applicable to reactor design, but to provide a reference for future development of design equations as more data is made available.

Section 2 is a brief description of the ferritic alloys which will be considered in this paper. The general strategy for handling a limited data base is presented in section 3. Sections 4, 5 and 6 are reviews of design equations for swelling, embrittlement, and irradiation creep respectively [4,9,16]. In section 7, a complete analysis of empirical and phenomenological thermal creep equations is provided. Included in this description is an application to material design criterion for ferritic steels based on thermal creep limitations. The summary and conclusions are stated in section 8.

2. Alloys

The alloys considered in this paper are ferritic steels of varying chromium and molybdenum concentration. The molybdenum is added as an alloying element to give carbon steels additional creep strength [5]. Low chromium addition improves the ductility, and higher concentrations of chromium help increase the oxidation resistance for temperatures up to 500–600°C [6]. Several specific ferritic alloys are analyzed in this paper including $2\frac{1}{4}$ Cr–1 Mo [5], Japanese HCM9M (9 Cr–2 Mo) [7], and Sandvik HT-9 (12 Cr–1 Mo) [8]. The last alloy is of particular

0167-899x/85/$03.30

interest for fusion reactor environments due to its high creep strength at higher operating temperatures and will be considered in more detail in this paper.

3. General data fitting

The difficulty in determining accurate design equations is the experimental data scatter and lack of sufficient data. In dealing with this limitation it is common in empirical descriptions of data to adopt standardized fitting forms. These include, for example, polynomial expressions, exponential and power fits and combinations of all three. Fitting data on an empirical basis may limit the applicability to within the data boundaries. On the other hand, theoretically-based equations may not be accurate enough to satisfy the needs of designers to predict certain phenomenon. In application to data produced during irradiation, it is necessary in some cases to consider at least partially theoretically-based models [9].

In handling the limited data base for empirical models, it is found that the technique of least squares is an efficient method to fit the data. This procedure can be applied to nonlinear equations for several cases as well as polynomial and other linear equations. Least squares is also useful for determining coefficients for phenomenological design equations.

For some empirical correlations the quantities to be fitted are based on parameters which are in turn functions of standard fundamental parameters such as stress and temperature. It is found that relating a quantity to these parameters may be more accurate, due to the potential large scatter of the data. For example, it will be shown in section 7 that the time to 1% creep strain is a smoother function of the time to creep rupture (which is a function of stress and temperature) than of stress and temperature independently.

In other data fits it is common to draw a band around widely scattered data and perform a linear or polynomial fit with the accepted error margin. This can be useful for predicting values of the ordinate outside the limits of the corresponding abcissa. Uncertainties in generating accurate interpolated values, however, can be a limiting factor for design purposes. Compressing the axes, i.e., fitting the logarithm of the quantities in question provides a more accurate fit where an empirical functional form is needed. The effort to tighten a data fit using this particular technique, however, can lead to problems in extrapolating outside the limits of the abcissa.

To fit sparse irradiated data for specific metals, one method of extrapolation is to use data from compositionally similar materials. Varying the composition concentration and normalizing similar data points can help fill in gaps in the data and complete design equations. The problem with this technique, however, is that a particular phenomenon which is characteristic of a specific material composition may not be characteristic of a similar but different composition.

It is clear that in applying one particular type of fit to determine an appropriate design equation, there will always be a compromise in some aspect of accuracy. The specific application of that design equation can define its desired limitation, and exceeding the bounds of the equation can lead to unexpected uncertainties. The reasons for choosing a particular data fit will therefore be discussed as they apply to the phenomena which will be described in subsequent sections.

4. Swelling

Fast reactor irradiation experiments have shown that low swelling is a phenomenon characteristic of ferritic steels. It is found [10] that the swelling behavior of ferritic alloys can be divided into three material categories: (a) pure iron and mild steels; (b) binary iron–chromium alloys; and (c) commercial ferritic and martensitic steels.

Analyzing the information on swelling for binary iron–chromium alloys may provide an insight into the swelling behavior of commercial alloys, as well as provide a suitable equation which can be adapted to data on commercial ferritics. The binary iron–chromium alloys exhibit well defined swelling peaks following irradiation to 30 dpa at temperatures in the range of 380°C–460°C [10]. The peak swelling temperatures are found to be essentially independent of chromium concentration and coincident with the equivalent peak present in pure iron. The magnitude of the swelling is a function of the chromium concentration, with a minimum around a chromium content of 5%.

For these alloys it is found that an increase in the swelling begins at a relatively low incubation dose. The swelling is proportional to a low power of the fluence, between $\frac{1}{2}$ and 2. The temperature dependence of the swelling is roughly Gaussian, with a shift in the peak swelling temperature for increasing dose rate. The compilation of neutron and ion irradiation

data for these alloys [10–13] have led to an expression for void swelling which was developed by Ghoniem [4].

$$\frac{\Delta V}{V_0}(\%) = \exp\left\{-\left(\frac{T-T_p}{W}\right)^2\right\}\{a\delta - b\}\{\phi(r)\}, \quad (1)$$

where $a = 0.036$, $b = 0.074$, and $W = 59°C$.

$$\phi(\mathrm{Cr}) = \begin{cases} 0.067(\mathrm{Cr})^2 - 0.457(\mathrm{Cr}) + 1.0 & (\mathrm{Cr} < 5\%) \\ 0.037(\mathrm{Cr}) + 0.237 & (\mathrm{Cr} > 5\%), \end{cases} \quad (2)$$

where Cr = chromium concentration.

$$T_p(°C) = 420 + 7.27 \ln(P(\mathrm{dpa/s})/10^{-6}). \quad (3)$$

For commercial ferritic and martensitic alloys, the swelling has been found to be insignificant below doses of 30 dpa [10]. Current work on swelling correlations indicates that there is apparently a large incubation dose, anywhere from 40 to 100 dpa for some alloys, below which there are no detectable voids. For alloys such as HT-9 a modification of the previous equation can account for the incubation dose if we adjust the constants a and b accordingly.

An alternative equation which has been used in several places [14,15] to describe void swelling is the following:

$$\frac{\Delta V}{V_0} = R\left\{\phi t + \frac{1}{\alpha}\ln\left[\frac{1+\exp[\alpha(\tau-\phi t)]}{1+\exp[\alpha t]}\right]\right\}, \quad (4)$$

where R is a function of temperature, α and τ are materials constants. This is a bi-linear equation, and it represents the proper fitting of the swelling for these ferritic steels, for it includes the provision for an incubation dose. The constants α and τ can establish the threshold temperature at which the swelling rate significantly increases.

Gelles and Puigh have recently applied this bi-linear equation to describe the swelling rate of $2\frac{1}{4}$ Cr–1 Mo [16]. The data were obtained by irradiating specimens to a peak fluence of 2.4×10^{23} n/cm^2 for temperatures from 390°C–560°C. The swelling equation includes a contribution from material densification, D, and the bi-linear term, S_0, which is identical to the swelling in eq. (4). The overall swelling is

$$\Delta V/V_0(\%) = S_0 - D, \quad (5)$$

where

$S_0 = \Delta V/V_0$ from eq. (4),

$$D = D^*[1 - \exp(-\lambda\phi t)], \quad (6)$$

τ swelling incubation parameter

$$[= C_1 \exp[C_2(T - C_3)^2]], \quad (7)$$

$R = 0.25\%/10^{22}$ n/cm^2,
α swelling rate $[= 0.5\ (10^{22}\ \mathrm{n/cm^2})^{-1}]$,
C_1 transition parameter,
$C_2 = 2.0 \times 10^{23}$ n/cm^2,
$C_3 = 5.0 \times 10^{-5}$ (K)$^{-2}$,
$T = 663$ K,
D^* steady state density $[= -0.08\%]$.
λ transition parameter $[= 3\ (10^{22}\ \mathrm{n/cm^2})^{-1}]$.

Please refer to ref. [16] for further discussion of the swelling phenomenon.

To date, no experiment exists which simulates exactly the fusion environment for the testing of materials. Helium is generated in materials by nickel doping and fast reactor irradiation to produce alpha particles. It has yet to be seen how the fusion environment affects τ and R, and until then, this correlation represents the best estimate of the effect of irradiation on swelling.

5. Embrittlement

One of the most serious concerns is the embrittling effect of neutron irradiation, because it produces brittle fracture in most metals, even at relatively high temperatures. A measure of brittle fracture is the transition temperature from low energy absorption, brittle fracture to high energy absorption, ductile rupture. The ductile-to-brittle transition temperature can be defined as the temperature at which the fracture stress intersects the yield stress on a stress vs. temperature diagram (fig. 1).

A more accurate measure of the embrittlement may be the fracture toughness, which can be related to the shift in DBTT. This value is geometrically defined as (see fig. 1)

$$\Delta\mathrm{DBTT} = \frac{\Delta\sigma_{10} - \Delta\sigma_{y0}}{(\partial\sigma_y/\partial T)}. \quad (8)$$

The factors that lead to a shift in the DBTT are numerous, and as such may be difficult to incorporate completely accurately into a general design equation.

The problem of fitting experimental data to physically-based design correlations has been treated by Odette [9]. He considered a description of embrittlement that is based partially on empirical models, and partially on phenomenological processes. The advantage of such a model is to predict the ΔDBTT at other fluences and temperatures for a given material without changing other parameters.

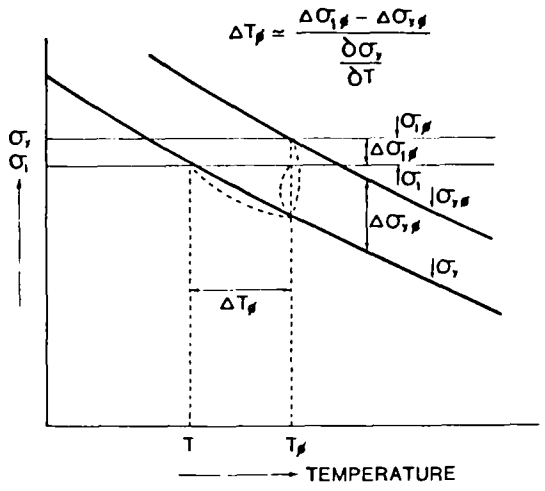

Fig. 1. Schematic illustration of shift in DBTT σ_y = yield stress, σ_i = fracture stress, ϕ = fluence, and ΔT is DBTT shift.

The phenomenon of embrittlement can be divided into several physical processes. The first is point defect production of vacancies and interstitials through displacement cascades caused by neutron–atom interaction. These defects may then form secondary defects such as vacancy clusters, dislocation loops, or precipitates [17]. The final effect is hardening due to dislocation–obstacle interaction. Analyses of the contribution of such defects to hardening have been experimentally investigated by Pachur [17] and theoretically by Ghoniem et al. [18]. It is also recently shown that copper vacancy complexes may be responsible for embrittlement of pressure vessel steels.

Translating these processes into physical terms, the first process, the defect production rate, is a function of:

1. the initial rate of atom displacement, C_1;
2. short-term thermal processes which determine effective production of dislocation obstacles, $C_2 f(T)$.

This production rate is:

$$G(t) \propto \phi\Sigma[C_1 + C_2 f(T)], \tag{9}$$

where $\phi\Sigma$ is the rate at which defects are being produced. The temperature dependence of the thermal processes is customarily chosen to be some form of a Gaussian function. Experimental evidence [19,20,21] has shown that this dependence accurately represents the functional description of the ductile to brittle transition in ferritic steels. If all parameters excluding dose and temperature are treated as constants for a particular material, the shift in DBTT is

$$\Delta\text{DBTT} = C\{1 - \exp[-C'\delta[C_1 + C_2 f(T)]]\}^m, \tag{10}$$

where $m = 0.5$.

The following design equation has been developed [4] for the shift in DBTT, and is based on hardening theories [22] similar to the one previously discussed:

$$\Delta\text{DBTT} = \frac{1.87 \times 10^4}{T - 238}\left\{1 - \exp\left[-\left(\frac{4T - 350}{T}\right)\delta^{1/2}\right]\right\}, \tag{11}$$

where δ = dose.

The equation is valid above approximately 250°C, below which the expression deviates from the ΔDBTT [17].

The effects of the steel composition, heat treatment, and the type of steel are not included in this formulation. It is also assumed for this equation that the ΔDBTT is 0°C before irradiation. The initial DBTT is normally affected by composition and heat treatment. These formulations are good for predicting ΔDBTT at other temperatures and fluences given data for a particular steel, but more work has to be done to incorporate compositional and other effects into the design equation.

Other forms of embrittlement in ferritic alloys are not treated in this paper. One important embrittling effect is temper embrittlement due to sulphur, phosphorous, and antimony. The phenomenon of temper embrittlement has been shown to be empirically related to the so called 'Watanabe number'. This number, which is a function of the concentrations of the previous elements, has been correlated to the degree of embrittlement through the Fracture Appearance Transition Temperature (FATT). Such an effect should be independently assessed in design procedures.

6. Irradiation creep

The limited available data on in-reactor creep for ferritic alloys has led to a simplified design equation [23]:

$$\epsilon_i = A_C \cdot \sigma\delta, \tag{12}$$

where A_C is a constant, σ is the applied Von Mises (equivalent) stress, and δ is the irradiation dose. In this equation, the data compiled from an experiment

[24] was used to determine the coefficient A_C. Due to the uncertainty in the experimental data scatter, the constant A_C was found to be in the range 7×10^{-7} dpa^{-1} ksi^{-1} to 2×10^{-5} dpa^{-1} ksi^{-1}. This equation was used for design studies which determined the lifetime of a blanket for a mirror machine [1].

Fortunately, more data has been compiled since then, specifically for $2\frac{1}{4}$ Cr–1 Mo [16]. The creep data were determined by irradiating specimens to a peak fluence of 5.7×10^{12} n/cm^2 for temperatures from 390°C–560°C. These data have been incorporated into a correlation developed by Gelles and Puigh [16], which describes the irradiation contribution to creep by two terms; (1) the irradiation creep, and (2) the swelling enhanced irradiation creep:

$$\epsilon_1 = \bar{B}\sigma^n \phi t + DS\sigma , \tag{13}$$

$\bar{B} = 0.4 \times 10^{-4}$ (MPa)$^{-1}$ (10^{22} n/cm^2)$^{-1}$ (%),
σ = effective stress (MPa),
S = fractional swelling rate (% per 10^{22} n/cm^2),
ϵ_1 = effective creep strain,
D = swelling enhanced creep coefficient [$= 2.7 \times 10^{-5}$ (MPa)$^{-1}$ (10^{22} n/cm^2)],
$n = 1.5$.

The first term is similar to the previous creep correlation (eq. (12)), and the second term, the swelling enhanced creep, is simply proportional to the swelling rate.

7. Thermal creep

The large available data base on thermal creep has led to this extensive development of creep related laws and design equations. Since much work has been done to orient the results of thermal creep testing to design applications, motivation for determining which fit to use will be discussed in detail.

7.1. Creep data base

Data collected from the various sources include various heat treatments and chemistry variations of the ferritic steels to be studied. The effects of these variations will not be analyzed in this section, for this is intended to be a statistical survey. The mechanical quantities in question are instead averaged over the various treatments, and the deviation in properties is treated as a contribution to the uncertainty of a particular quantity. This allows a broader application of the design equations to various systems without seriously considering variations in chemical composition or heat treatment. As a matter of consequence, the deviation in the aforementioned quantities is small enough to warrant application of this procedure.

We therefore consider two classes of creep data. The first is information on creep rupture life as a function of operating temperature and stress. Data of this type is used to determine the allowable design stress [25] at a given temperature and desired lifetime. Creep rupture data is available for the ferritic steels discussed in the introduction [5,7,8].

The second class of data is information on elongation vs. time. The results of specific creep tests at three temperatures were provided by Sandvik Steel Research Center [8] on the ferritic steel HT-9. Data on 1% strain, 5% strain, and elongation to fracture are useful for the development of the design equations for elongation vs. time. Data on elongation vs. time for $2\frac{1}{4}$ Cr–1 Mo consist of several creep curves which identify a multitude of creep phenomena which will be discussed further on.

One final class of information to be used for design purposes is the ultimate tensile strength. Data for the three ferritic steels [26,7,27] can be used together with creep rupture data to determine design criterion.

7.2. Empirical laws for creep deformation

While the available data for creep rupture and creep strain go up to 2–5 years, many designs required service lives greater than 30 years. This is the motivation for utilizing empirical type equations which allow a degree of freedom in extrapolating the material lifetime, while limiting the range of applicability in the temperature dimension. These empirical equations are accurate in a limited yet important range.

7.2.1. Creep rupture

There is no universally acceptable "standard" method for extrapolating creep rupture data to longer design lives. In a review of available methods. LeMay [28] considered five different functional forms for creep rupture data. The representation of this data using a particular form is achieved by considering plots of log t_r, where t_r is the rupture time, versus the temperature T or its inverse for different stresses.

Each equation is based on the convergence or divergence of the isostress lines, and hence there exist several functions which describe creep rupture phenomena for different conditions. As a result, the Minimum Commitment Method, a general for-

mulation [29], was developed in 1971 for NASA to avoid forcing data through a set pattern. The equation based on this method has the following form:

$$\ln t_r + AP(T) \ln t_r + P(T) = G \ln \sigma_r . \tag{14}$$

For the application of creep data for ferritic steels which are possible candidates for fusion reactor designs, Ghoniem [30] has developed a general design equation which is a modified form of the Minimum Commitment Method. The available data best fits the curvature defined by the following functional forms:

$$\ln \rho_r = K(T) - \frac{1}{m(T)} \ln t_r , \tag{15}$$

$$K(T) = \sum_{i=0}^{2} a_i T^i , \tag{16}$$

$$m(T) = \sum_{i=0}^{2} b_i / T^i . \tag{17}$$

For HT-9, $2\frac{1}{4}$ Cr-1 Mo, and HCM9M the coefficients for average rupture stress vs. rupture time were determined using least squares. These are listed in tables 1–3. Figs. 2 and 3 are comparisons of the data and curves fit for HT-9 and $2\frac{1}{4}$ Cr-1 Mo respectively.

Table 1
HT-9
Coefficients for rupture time vs. stress

$a_0 = 138.4149302$	$b_0 = -1531.358687$
$a_1 = -0.3233496513$	$b_1 = 2506695.289$
$a_2 = 1.946588668E\text{-}4$	$b_2 = -1017186681$

Table 2
$2\frac{1}{4}$ Cr-1 Mo
Coefficients for rupture time vs. stress

$a_1 = -5.29241542$	$b_1 = 95.7285956$
$a_2 = 2.949030167E\text{-}2$	$b_2 = -1.65807074E5$
$a_3 = -2.189875519E\text{-}5$	$b_3 = 7.794222884E7$

Table 3
HCM9M
Coefficients for rupture time vs. stress

$a_1 = -13.70067744$	$b_1 = 86.7029448$
$a_2 = 0.0470486378$	$b_2 = -1.757071356E5$
$a_3 = -3.084945533E\text{-}5$	$b_3 = 9.29956477E7$

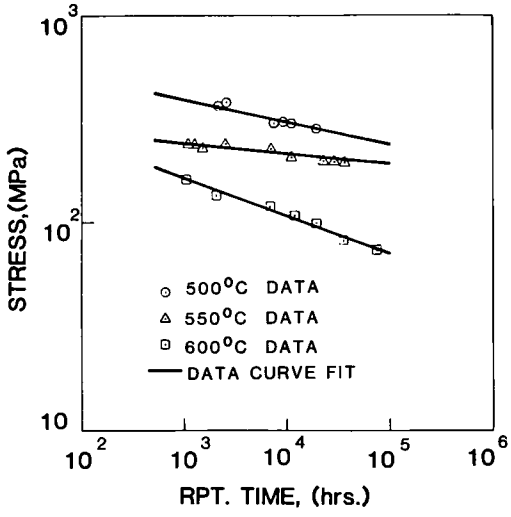

Fig. 2. HT-9 stress vs. rupture time.

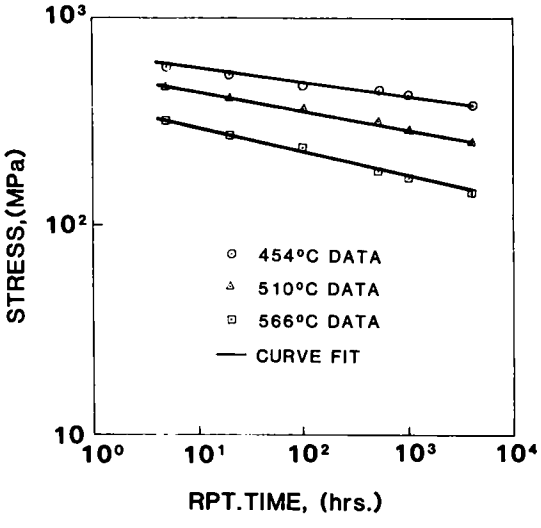

Fig. 3. $2\frac{1}{4}$ Cr-1 Mo stress vs. rupture time.

7.2.2. Ultimate tensile strength

This property is not classified under creep deformation, but it can be used as a limit for material design for a wide temperature range. It is found that a cubic equation is sufficient to accurately determine the average ultimate tensile strength as a function of temperature:

Table 4
HT-9
Ultimate tensile strength

$c_1 = 299.7297993$
$c_2 = -1.118150821$
$c_3 = 1.98126826E\text{-}3$
$c_4 = -1.179135173E\text{-}6$

Table 5
$2\frac{1}{4}$ Cr–1 Mo
Ultimate tensile strength

$c_1 = 152.7886198$
$c_2 = -0.59380158$
$c_3 = 1.437869976E\text{-}3$
$c_4 = -1.060565681E\text{-}6$

Table 6
HCM9M
Ultimate tensile strength

$c_1 = 132.2272634$
$c_2 = -0.257205081$
$c_3 = 4.244588867E\text{-}4$
$c_4 = -2.732474633E\text{-}7$

$$\bar{\sigma}_{\mathrm{UTS}} = \sum_{i=0}^{3} c_i T^i \,. \tag{18}$$

The coefficients are listed in tables 4–6.

7.2.2. Elongation vs. time

The creep data supplied by Sandvik [8] includes elongation curves for three temperatures; 500, 550 and 600°C. These figures are characterized by the primary, secondary, and tertiary regions common to creep strain vs. time curves. Material design often necessitates the use of information on strain and strain rates of materials under applied loads. Usually a value of strain is chosen as a maximum limit for acceptable deformation, and this value occurs well before the onset of tertiary creep. The following is a description of elongation vs. time for the three regions of creep. This set of equations can be placed directly in a computer code for determining time-dependent strain histories between 500 and 600°C. The main purpose of this description, however, is to supply a means for evaluating strains for other conditions based on a limited data base.

In particular, the values of time to 1% strain, 5% strain, and creep rupture were provided for different melts of HT-9, in addition to the creep curves [8]. Several characteristics identifiable on creep curve can therefore be used to extrapolate incomplete data. For example, it is found that the 1% strain falls in the primary region or at the beginning of the secondary region. The 5% strain is on the borderline of the secondary–tertiary boundary, or well into the tertiary region. These data points are therefore situated at a good position to interpolate a secondary region between them.

The primary and secondary regions can be coupled to form one equation, even though it is standard to represent the secondary region by a linear form. In this region, it is necessary to use as many points as possible to accurately describe the curvature. It is for this reason that the times to 1% and 5% strain are used to model a two-point exponential form representative of the primary-secondary region. In addition, it is in this region that design limitations for creep strain deformation are usually set, so the equation for this region can be used alone if it is desired for design purposes.

Since the 5% strain at times falls well into the tertiary region, this particular portion of the curve is fit to a one point exponential. Extrapolating to $0.9 * t_5$, where t_5 = time to 5% strain, provides a point in the secondary region. This point coupled with the 1% strain point is fitted to the following form:

$$\epsilon(t) = [1 - \exp(bt^{\alpha})] \times 100\% \,, \tag{19}$$

which is similar to the creep strain equation of McVetty [31]:

$$\epsilon = a + bt + c\exp(-dt) \,. \tag{20}$$

The constants b and α of eq. (19) are fit in the following manner (t_1 = time to 1% strain):

$$t' = 0.9 t_5 \,, \tag{21}$$

$$a = \ln 5/t_5^2 \,, \tag{22}$$

$$\epsilon_2 = 0.01 \exp(at'^2) \,, \tag{23}$$

$$\alpha = \ln(\ln(1-\epsilon_2)/\ln(1-\epsilon_1))/\ln(t'/t_1) \,, \tag{24}$$

$$b = \ln(1-\epsilon_1)/t_1^{\alpha} \,, \tag{25}$$

here a, $\alpha > 0$ and $b < 0$. This fit is good for $0 < t < t'$.

In the region between t' and t_5, the fit is determined by eqs. (21)–(23), with the expression:

$$\epsilon(t) = \exp(at'^2) \quad (\%) . \tag{26}$$

Finally, in the tertiary–rupture region, the fit is an exponential of the following form:

$$\epsilon(t) = \exp(ct^{\gamma}) \quad (\%) , \tag{27}$$

where

$$\gamma = \ln(\ln \epsilon_R / \ln \epsilon_5)/\ln(t_r/t_5) , \tag{28}$$

$$c = \ln(\epsilon_R)/t_r^{\gamma} , \tag{29}$$

$\epsilon_5 = 5\%$ strain, ϵ_R = rupture strain. This fit is good for $t_5 < t < t_r$.

The entire creep strain curve can therefore be constructed from points t_1, t_5, and ϵ_R. These points are functions of temperature and applied stress.

The data supplied by Sandvik on t_1, t_5, and ϵ_R are not consistent functions of stress. It is found that these points are more consistently functions of the rupture time, which is a function of temperature and stress. Eq. (15) can be written in terms of the rupture time:

$$t_r = \exp(m(T)K(T))/\sigma^{m(T)} , \tag{30}$$

with the same coefficients $K(T)$ and $m(T)$. The stress in eq. (30) is the applied stress.

The time to 1% strain is found to best fit the rupture time by the following form:

$$\ln t_1 = J(T) \ln t_r + L(T) , \tag{31}$$

$$J(T) = \sum_{i=0}^{2} J_i T^i , \tag{32}$$

$$L(T) = \sum_{i=0}^{2} L_i T^i . \tag{33}$$

and the coefficients J_i and L_i are listed in table 7. This form is an example of the compression of the axes by fitting the logarithm of the quantities.

The time to 5% strain is fit to a polynomial function of both temperature and rupture time:

$$t_5 = \sum_{i=0}^{2} \sum_{j=0}^{2} a_{ij} T^j t_r^i , \tag{34}$$

with coefficients a_{ij} found in table 8. Since the data for time to 5% strain is a relatively consistent function of rupture time, a simple polynomial is used for the data fit. A cubic fit was chosen because it has a small number of coefficients, but is more accurate than a quadratic fit.

Finally, the rupture strain, ϵ_R, is found to roughly fit the rupture time in the following form:

$$\ln \epsilon_R = n(T) \ln t_r + p(T) , \tag{35}$$

Table 7
HT-9
Coefficients for t_1 vs. rupture time

$J_0 = -119.4828446$	$L_0 = 1707.558058$
$J_1 = 0.2860065163$	$L_1 = -4.091847968$
$J_2 = -1.687029056\text{E-}4$	$L_2 = 2.435742087\text{E-}3$

Table 8
HT-9
Coefficients for t_5 vs. rupture time

$a_{00} = 5.800800737\text{E}4$	$a_{12} = -4.906002324\text{E-}6$
$a_{01} = -142.9532355$	$a_{20} = 1.275428065\text{E-}3$
$a_{02} = 8.746716625\text{E-}2$	$a_{21} = -2.979495964\text{E-}6$
$a_{10} = -2.257160655$	$a_{22} = 1.74509467\text{E-}9$
$a_{11} = 7.669299551\text{E-}3$	

Table 9
HT-9
Coefficients for elongation vs. rupture time

$n_0 = 54.32308035$	$p_0 = -465.7071298$
$n_1 = -0.1286025719$	$p_1 = 1.110624330$
$n_2 = 7.581206028\text{E-}5$	$p_2 = -6.547203129\text{E-}4$

$$n(T) = \sum_{i=0}^{2} n_i T^i , \tag{36}$$

$$p(T) = \sum_{i=0}^{2} p_i T^i . \tag{37}$$

The coefficients n_i and p_i are in table 9. The final form of the creep strain as a function of stress and temperature is represented by the following equation:

$$\epsilon = f\{t_1(t_r(\sigma, T), T), t_5(t_r(\sigma, T), T), t_r(\sigma, T), \epsilon_R(t_r(\sigma, T), T)\} . \tag{38}$$

7.3. Material design

The ASME Code Case 1592 for Class 1 Components in Elevated Temperature Service [32] provides design criteria for structural components at temperatures characteristic of thermal creep. The code assigns a different allowable stress for each stress classification. Table 10 lists the structural design criteria as per ASME code specifications for the stress intensity factor S_{mt}. At lower temperatures S_{mt} is typically a frac-

Table 10
Design allowable stresses from ASME code case N-47

Time-independent allowable stress, S_m (other than bolting)	Lowest value of	1/3 S_{ult} at room temperature 1/3 S_{ult} at temperature 2/3 S_y at room temperature 2/3 S_y at temperature
Time-dependent allowable stress, S_t	Lowest value of	2/3 of minimum stress to cause creep rupture in time t 80% of minimum stress to cause tertiary creep in time t Minimum stress to produce 1% strain in time t
General primary-membrane allowable stress S_{mt}		Lesser of S_m and S_t at temperature and time

S_{ult} = ultimate strength.
S_y = yield strength.

tion of the ultimate tensile strength. At higher temperature S_{mt} is characteristic of a fraction of the stress to cause creep rupture.

In particular, for the three ferritic steels, it is found that the criterion which satisfies the minimum of the stress intensity factor is the minimum of the following: 33% of the minimum ultimate tensile strength at $T+10\%$, or 67% of the minimum stress to cause creep rupture. The first of these is approximately equal to $\frac{1}{3}$ of the average ultimate tensile strength. The design criteria for the three steels is shown in figs. 4–6. It may be noted that after about three years the design curve for structural components based on the ASME code saturates. Fig. 7 is a comparison of the design criteria for the three steels for a design lifetime of three years. It is seen that although HT-9 represents the superior steel from a design standpoint, $2\frac{1}{4}$ Cr–1 Mo cannot be counted out as a potential structural material.

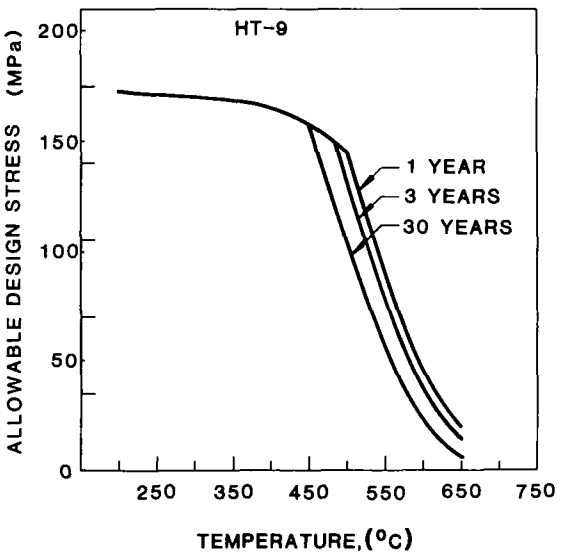

Fig. 4. HT-9 design stress based on ASME code.

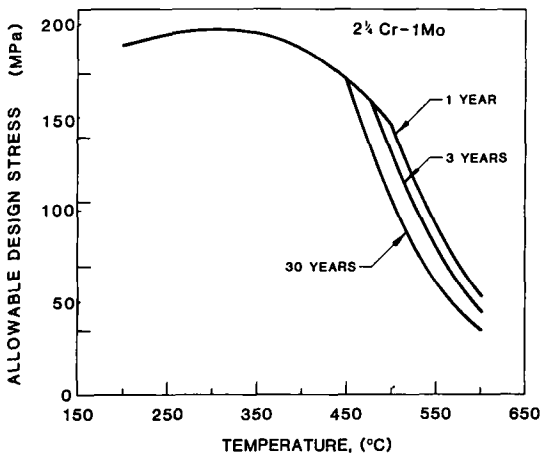

Fig. 5. $2\frac{1}{4}$ Cr–1 Mo design stress based on ASME code.

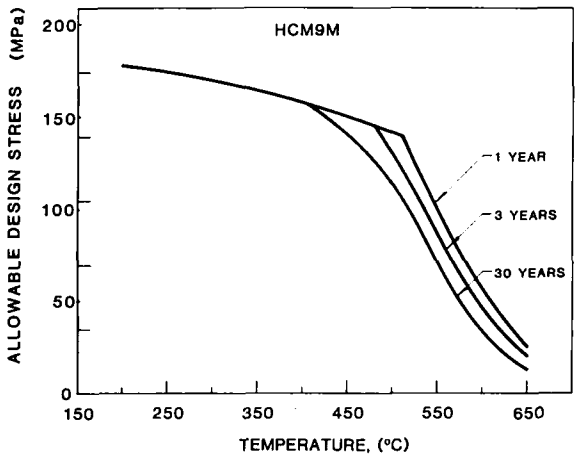

Fig. 6. HCM9M design stress based on ASME code.

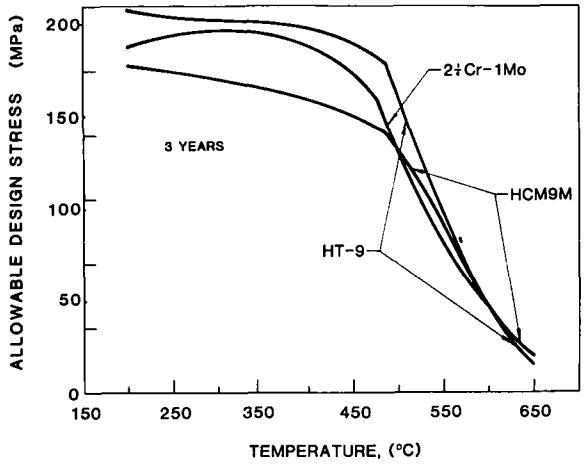

Fig. 7. Comparison of design stresses for three year lifetime.

7.4. *Uncertainty analysis*

For the material design curves, the error is based on the computed rupture stresses as a function of rupture time. The range of any particular creep rupture curve occurs in a small band of deviation of the stress on the ordinate. The maximum of the average errors in rupture stress for any particular temperature for the three steels is about 8%.

In determining the rupture time vs. rupture stress, however, it is important to note that the rupture time covers five orders of magnitude or more on the abcissa (figs. 2 and 3). Thus, errors on a log scale for calculating the rupture time vs. stress may translate into orders of magnitude on a linear scale. Therefore, a given stress level can only provide a fair but reasonable estimate of the time to rupture, based on the nature of the data. This amounts to about 20–30% error in rupture times for the given stress and temperature.

The average ultimate tensile strength for some of the steels was determined by taking the average of several values of UTS found in the references. The cubic equation is an accurate fit for these values, and the error never exceeded 5% of any curve.

The next issues of concern for accuracy are the data points for 1% and 5% strain times and the overall creep strain curve. There is considerable error in the functional determination of times to 1% and 5% strain, as much as 50%. The data spread is so wide for these two particular times as a function of stress that such a deviation is expected. In addition, these characteristic times depend upon the accuracy of the determination of rupture time. In spite of these differences, the primary and secondary regions were fit with reasonable accuracy to the data, as can be seen in fig. 8.

The tertiary and rupture regions are generally underestimated, as seen in the figures. This can amount to an error of about 20%–30% or more in some cases. In general it can be said, however, that the overall form of the creep strain curve is preserved with a certain degree of accuracy.

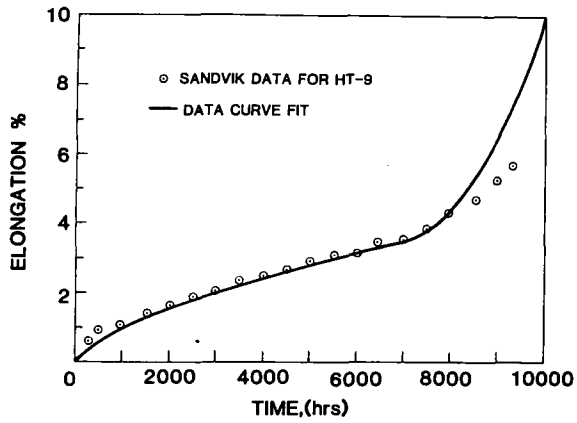

Fig. 8. HT-9 elongation vs. time for $T = 600°C$ and stress = 106 MPa.

Finally, it should be noted that the elongation to rupture correlation was used to obtain a very rough estimate of this parameter, and that the data spread was so bad that no correlation can truly be depended upon for strict accuracy. For determining the creep rupture curves, however, the fit of elongation versus rupture time has been found to be sufficient for determining the curve structure.

7.5. Range of applicability

The determination of minimum stress vs. rupture time included a graphical extension of the curves outside the temperature data range. Although this was necessary to construct the material design curves, the calculation of average stress vs. rupture time and vice-versa should not exceed the temperature bounds. For HT-9, this limits the temperature range to 500–600°C, for $2\frac{1}{4}$ Cr–Mo, 450–575°C, and for HCM9M, the range is 450–700°C.

The ultimate tensile strength for all three metals is valid for 200–600°C.

For the determination of the HT-9 creep strain vs. time curves, the upper and lower limits of the stress in ksi versus temperature in K are given by:

$$\sigma_u = -T/5 + 202.63 \text{ ksi}, \tag{39}$$

$$\sigma_b = -T/5 + 189.63 \text{ ksi}. \tag{40}$$

7.6. Steady-state creep rate

In the previous empirical descriptions of creep phenomena, data fitting was utilized which more or less attempted to preserve the overall shape of any particular curve. In these cases accuracy was optimized without specific regard to the physical basis behind the application. The dependence of the steady-state creep rate on applied stress and temperature, however, can be analyzed by application of data to an Ashby-type deformation map [33]. In this description, the dominant deformation mechanisms are displayed as a function of stress and temperature.

In particular, it is found that for HT-9 the phenomenon of dislocation creep is characteristic of the data supplied by Sandvik Laboratories. Although this conclusion is based on a limited amount of data, it provides a means to obtain an understanding of the phenomena which may be taking place in a material during deformation. It also supplies a reasonable fit of the data which is more physically plausible than an arbitrary functional form. Steady-state dislocation creep is a consequence of the competing effects of strain hardening and thermal softening in balance. This mechanism involves the climb and glide of dislocations by means of stress-assisted vacancy movement, and is described by phenomenological expressions such as [34]

$$\dot{\epsilon} = A\sigma^n \exp(Q_c/RT), \tag{41}$$

and [28]

$$\dot{\epsilon} = B(D_v Gb/KT)(\sigma/G)^n, \tag{42}$$

which are identical since D_v = self-diffusion coefficient:

$$D_v \propto \exp(-Q_c/RT), \tag{43}$$

and Q_c is the activation energy for self-diffusion.

It is found that for most pure metals n is usually in the range of 3–6, but in dispersion hardened alloys, the values of n and Q_c have been found to be significantly higher. Some examples of this include TD nickel [35], where n can be as high as 40, compared to pure nickel where $n = 5$, and Nimonic 80A [36] where $n = 8.3$, compared with a value of $n = 5$ for the nickel –20% chromium matrix material.

To explain this anomalous behavior, it has been suggested [34] that the creep takes place under the influence of an active or effective stress $(\sigma - \sigma_0)$ where σ is the applied stress and σ_0 is the friction stress which the dislocation must overcome to move through the lattice. This overall process is governed by the glide of dislocations controlled by viscous drag by solute atoms or second phase particles. The stress is analogous to the parameter found in the relationship between the applied stress and the density of dislocations not associated with subgrain boundaries, i.e.,

$$\sigma = \sigma_0 + \alpha\mu b\sqrt{\rho}, \tag{44}$$

where α is a constant, μ is the shear modulus, b is the Burger's vector, and ρ is the dislocation density. The stress $(\sigma - \sigma_0)$ therefore determines the rate of recovery and the creep rate.

A more concise derivation [28] reveals that the dependence of creep rate on temperature and stress can be represented by the following form, due to the process of dislocation creep:

$$\dot{\epsilon} = (16\pi^3 D_v bc_j/G^2KT)(\sigma - \sigma_0)^n, \tag{45}$$

where c_j = concentration of jogs, $n = 3$–4, and in this formulation, $\sigma_0 = Av/b$, where v = velocity of mobile dislocations, and A = temperature dependent time constant. At the present, work is in progress to construct a phenomenological dislocation creep model.

This will extend the data to complex loading conditions, and will allow the incorporation of radiation effects.

HT-9 creep equation

For HT-9, it is found that the above expression can be written as

$$\dot{\epsilon} = \frac{B}{kT}(\sigma - \sigma_0)^3 \exp(-Q^*/kT), \quad (46)$$

where $B = 7.385 \times 10^{-3}$, $Q^* = 1.23$ eV, $n = 3$, $k = 8.6207 \times 10^{-5}$ eV/K, and $\sigma_0 = aT + C$ ksi, where $a = -0.2185$ and $c = 198.1783$, T is in K and σ, σ_0 are in ksi. These constants were determined using least squares. The strain hardening exponent of 3 was found to optimize the minimum error for the data on HT-9.

The value of Q_c is close to the migration energy of vacancies, 1.2–1.3 eV, which may suggest that the dislocation creep mechanism in HT-9 is controlled by vacancy movement which is responsible for the glide of dislocations. This phenomenological formulation is good for the temperature range of 500°C–600°C and stress levels ranging from 12.5–50 ksi limited by eqs. (45, 46).

$2\frac{1}{4}$ Cr–1 Mo creep equation

The data on $2\frac{1}{4}$ Cr–1 Mo [37] indicate that the elongation vs. time cannot be simply divided into three regions. At some value of elongation in time, the secondary creep breaks off into a second steady-state creep region. This suggests that a bi-linear equation is a prime candidate for application to this data.

However, for design purposes, it is found that in a small temperature range, 370°C–470°C, the creep can be represented by a single secondary region up to a cumulative strain of 1%.

$$\dot{\epsilon} = \frac{B}{kT}(\sigma - \sigma_0)^4 \exp(-Q^*/kT), \quad (47)$$

where $\ln B = 17.2898$, $Q^* = 2.767$ eV, $n = 4$, $k = 8.6207 \times 10^{-5}$ eV/K, and $\sigma_0 = aT + C$ ksi, where $a = 51.7929$ and $C = -0.0628$.

The value of the applied stress should not exceed 40 ksi. This particular fit is sufficient to support design studies in that temperature range. Clearly more complicated processes occur in $2\frac{1}{4}$ Cr–1 Mo, and must be accounted for with the proper physical modeling.

This form of the steady state creep is similar to eq. (46), but the stress exponent of 4 was found to minimize the error. The reason for this may be that different processes are occurring in a different temperature regime from HT-9, considering the location of the material range on the Ashby deformation map. In any case the two eqs. (46) and (47) should not be compared. Future work on the phenomenological basis of thermal creep of $2\frac{1}{4}$ Cr–1 Mo may reveal a more physical understanding of the corresponding creep mechanism.

8. Summary and conclusions

In this paper we have discussed several methods for developing design correlations for several ferritic steels. A general strategy for handling a limited data base was reviewed, and several methods for fitting data empirically and theoretically were discussed. Design equations covering the phenomena of irradiation induced swelling, embrittlement and irradiation creep were reviewed from the literature. We developed a design equation for rupture time deformation of HT-9, as a function of applied stress and temperature for HT-9, $2\frac{1}{4}$ Cr–1 Mo, and HCM9M. We presented design equations for thermal creep deformation of HT-9 which cover the following properties:

1. Time to 1% strain as a function of stress and temperature.
2. Time to 5% strain as a function of stress and temperature.
3. Rupture strain as a function of stress and temperature.

In addition, the creep strain as a function of time, temperature, and stress was determined for HT-9. This includes the primary, secondary, and tertiary regimes of creep. The coefficients for the correlations should be carried out to as many digits as possible for increased accuracy. Also, the equations should not be used outside the range of applicability discussed in the report.

The HT-9 creep data in the range 500–600°C is found to represent behavior typically described by dislocation creep. The phenomenological equation used to represent the data is based on an effective stress acting on dislocations. The friction stress was found to be only a function of temperature. This approach indicates that dislocation climb is controlled by vacancy absorption at dislocations.

A design equation which has a similar

phenomenological basis was presented for the alloy $2\frac{1}{4}$ Cr–1 Mo. This equation was found to represent the thermal creep in a limited temperature range, 370°C–470°C, and a cumulative strain of 1%, due to the nature of the elongation vs. time. The correlation is valid up to an applied stress of not more than 40 ksi. The activation energy also indicates that vacancy absorption is responsible for dislocation climb.

References

[1] J.P. Blanchard and N.M. Ghoniem, The effect of irradiation and thermal creep on stress redistribution in fusion blankets, Third Topical Meeting on Fusion Reactor Materials, Albuquerque, 1983, J. Nucl. Mater. 122 & 123 (1984).

[2] R.L. Klueh, J.M. Vitek and M.L. Grossbeck, J. Nucl. Mater. 103–104 (1981) 887.

[3] R.L. Klueh and J.M. Vitek, J. Nucl. Mater. 117 (1983) 295.

[4] N.M. Ghoniem and R.W. Conn, Assessment of ferritic steels for steady state fusion reactors, International Atomic Energy Agency, Proc. on Fusion Reactor Design and Technology, IABA-TC-392/62, Vol. II (1983) p. 389.

[5] R.L. Klueh, Chromium–molybdenum steels for fusion reactor first walls: a review, Proc. of Conf. on Structural Materials in Reactor Technology, SMiRT-6, Paris, France, August 1981.

[6] J. Orr, F.R. Beckitt and G.D. Fawkes, The physical metallurgy of chromium–molybdenum steels for fast reactor boilers, in: Ferritic Steels for Fast Reactor Steam Generators, Vol. 1, British Nuclear Energy Society, London (1978), pp. 91–109.

[7] T. Yukitoshi et al., Application of 9 Cr–2 Mo steel (HCM9M) for fast breeder reactor steam generato's, The Sumitomo Search No. 23 (May, 1980).

[8] Data supplied by Dr. Thomas Anderson, Manager of the Product Development Section of Sandvik Steel Research Center.

[9] G.R. Odette et al., Analysis of Radiation Embrittlement Toughness Curves – Section 6, Fracture Control Corporation Progress Report FCC 78-11 (1978).

[10] E.A. Little and D.A. Stow, J. Nucl. Mater. 87 (1979) 25.

[11] E.A. Little and D.A. Stow, Metal Science 14 (1980) 89.

[12] R.D. Watson, R.R. Peterson and W.G. Wolfer, The effect of irradiation creep, swelling wall erosion, and embrittlement on the fatigue life of a tokamak first wall, Proc. of the Second Topical Meeting on Fusion Reactor Materials, August 1981, Seattle, WA.

[13] W. Daenner, A comparison of AISI 316 and German type DIN 1.4970 stainless steel with regard to the first wall lifetime, ibid.

[14] R.E. Mattas, Fusion component lifetime analysis, ANL/FPP/TM-160, Fusion Power Program (September 1982).

[15] J.F. Bates and M.K. Korenko, Empirical development of irradiation-induced swelling design equations, Nucl. Technol. 48 (1908) 303.

[16] D.S. Gelles and R.J. Puigh, Alloy development for radiation performance, Semi-Annual Progress Report, DOE/ER/0045/11 (September 1983).

[17] D. Pachur, NRC Seventh Water Reactor Conference, Gaithersburg, Md., Nov. 1979. Also: D. Pachur, American Nuclear Society Transactions, 38 (1981) 307.

[18] N.M. Ghoniem, J.N. Al-Hajji and F.A. Garner, Hardening or irradiated alloys due to the simultaneous formation of vacancy and interstitial loops, Effects of Radiation on Materials: Eleventh Conference, ASTM STP 782, (1982) pp. 1054–1072.

[19] G. Hofer and C.C. Hung, Nucl. Technol. 49 (1980) 492.

[20] G. Hofer and C.C. Hung, New criteria for Charpy impact testing of ferritic steels, Siemens Forsch. Entwicklungsber. 8 (1979) 69.

[21] G. Hofer and C.C. Hung, New criteria for Charpy impact testing of ferritic steels, Trans. Am. Nucl. Soc. 31 (1979) 584.

[22] M.J. Makin and F.J. Minter, J. Inst. Metals 85 (1957) 397.

[23] G.R. Odette, Property Correlations for Ferritic Steels for Fusion Applications, Damage Analysis and Fundamental Studies Information Meeting, October 2–3, 1980.

[24] E.R. Gilbert and B.A. Chin, In-reactor creep measurements, HEDL-SA-1403 (1978).

[25] N.M. Ghoniem, J. Blink and N. Hoffman, Selection of alloy steel type for fusion power plant applications in the 350–500°C range, Proc. of Topical Conference on Ferritic Alloys for Use in Nuclear Energy Technology, Snowbird, Utah, June 19–23, 1983.

[26] J.M. Rawls et al., Assessment of matensitic steels as structural materials in magnetic fusion devices, General Atomic Report GA-A15749 (January, 1980).

[27] R.L. Klueh and R.W. Swindeman, Metallurgical effects on the mechanical properties of $2\frac{1}{4}$ Cr–1 Mo, in: Ferritic Steels for Fast Reactor Steam Generators, BNES, London (1978), p. 100–114.

[28] I. LeMay, Principles of Mechanical Metallurgy (Elsevier, New York, 1982) p. 363.

[29] S.S. Manson and C.R. Ensign, NASA TM.X-52999 (1971).

[30] N.M. Ghoniem and R.W. Conn, High temperature evaluation of ferritic steels for fusion reactors, in: Papers Submitted for Presentation at the American Nuclear Society Meeting, PPG-612, Los Angeles, June 1982.

[31] P.G. McVetty, Mech. Engrg. 56 (1934) 149.

[32] ASME Boiler and Pressure Vessel Code, 1977 Code Cases – Nuclear Components, 1977 Edition, Case N-47

(1977) 1592-10.
[33] M.F. Ashby, Acta Met. 20 (1972) 887.
[34] J.D. Parker and B. Wilshire, Metal Science 9 (1975) 248.
[35] B.A. Wilcox and A.H. Clauer, Trans. Met. Soc. AIME 236 (1966) 570.
[36] D. Sidey and B. Wilshire, Metal Science 3 (1969) 56.
[37] C.E. Pugh, D.N. Robinson et al., Background Information for Interim Methods of Inelastic Analysis for High-Temperature Reactor Components, ORNL/TM-5226 (May 1976).